AIAA JOURNAL
Vol. 41, No. 3, March 2003

Dynamics of an Internal Flowfield Driven by Two Hydrodynamic Instabilities

Jérôme Vétel,* Frédéric Plourde,† and Son Doan-Kim‡
Ecole Nationale Supérieure de Mécanique et d'Aérotechnique, 86960 Futuroscope Cedex, France

Hydrodynamic instabilities in a confined flow generated by air injection through porous walls separated by an emerging obstacle are experimentally characterized. Two different mechanisms of instabilities have been detected: a vortex shedding phenomenon back to the obstacle location and one developing along the porous wall. The latter was found to provide most of the acoustic energy. Influence of an unbalanced mass flow rate between each side of the obstacle has been carried out over a wide range of mean velocities; an increase of the mass flow rate injected downstream of the obstacle implies resonance amplification by wall vortex shedding that strengthens the instabilities in the chamber. On the other hand, an increase in the mass flow rate upstream from the obstacle location favors vortex pairing and self-sustained oscillations, whereas acoustic wave generation by wall vortex impingement is weakened.

Nomenclature

a	=	sound velocity, m/s
f_{nL}	=	nth longitudinal acoustic mode, $na/2L$, Hz
h_c	=	channel height, m
h_t	=	height of the nozzle throat, m
It	=	turbulence intensity, $\sqrt{(\overline{u'^2} + \overline{v'^2})}/aM$
L	=	channel length, m
l	=	distance between the obstacle and the nozzle locations, m
M	=	characteristic Mach number based on the mass flow rate, $q_m/a\rho s$
p, p'	=	mean and fluctuating pressure at the head end, Pa
q_m	=	total mass flow rate, kg/s
q_0	=	mass flow rate of the first injecting block, kg/s
q_1	=	unbalanced mass flow rate at the first injecting block, kg/s
Re	=	Reynolds number, $q_m/w\mu$
$R_{x'y'}$	=	correlation coefficient of arbitrary functions of time x' and y', $x'(t) \cdot y'(t+\tau)/\sqrt{x'(t)^2}\sqrt{y'(t)^2}$
r	=	distance between two probes normalized by the channel height h_c
$S_{x'}$	=	power spectral density normalized by rms x' fluctuations, $s_{x'x'}/\overline{x'^2}$, Hz^{-1}
s	=	characteristic surface area, wh_c, m^2
$s_{x'y'}$	=	power spectral density, $\lvert s_{x'y'}\rvert e^{i\theta_{x'y'}}$
u_c	=	convection speed of coherent structures, m/s
u', v'	=	fluctuation velocity components in X, Y direction, m/s
w	=	channel width, m
X, Y	=	nondimensional axis normalized, respectively, by l and h_c
α	=	normalized unbalanced mass flow rate, $(q_1 - q_0)/q_m$
$\theta_{x'y'}$	=	phase angle, rad
μ	=	dynamic viscosity, kg/ms
ρ	=	density, kg/m^3
τ	=	time delay, s

Received 6 March 2002; revision received 14 October 2002; accepted for publication 31 October 2002.

*Scientist, Laboratoire d'Etudes Thermiques, Téléport 2, 1 Avenue Clément Ader, B.P. 109.

†Centre National de la Recherche Scientifique Researcher, Laboratoire d'Etudes Thermiques, Téléport 2, 1 Avenue Clément Ader, B.P. 109. Member AIAA.

‡Professor, Laboratoire d'Etudes Thermiques, Téléport 2, 1 Avenue Clément Ader, B.P. 109.

I. Introduction

SELF-SUSTAINED oscillations remain an important topic in flowfield dynamics. Generally, an impinging shear layer gives rise to noise radiation that drives through a feedback phenomenon the initial excitation of the shear layer at the separation point. Exhaustive studies have been conducted on this subject because the problem occurs in a large variety of flow configurations and industrial applications. The works of Rockwell and Naudascher[1] and Rockwell[2] provide an overview of experimental studies, as well as theoretical approaches on free impinging shear layers. When flow is established in a confined chamber, self-sustained oscillations can couple with acoustics, a fact which implies different resonance states. Many works have been conducted on flowfield in ducts containing sets of obstacles[3–5] and flow over cavities.[6–8] In these cases, coherent structure shedding generated at geometric discontinuities can match up with an acoustic mode of the chamber, and the coupling phenomenon induces different types of oscillation behavior mainly characterized by frequency stages, which depend on separation to impingement length and mean flow velocities. Rossiter[9] analyzed this mechanism by a change in the number of vortices in the shear layer. His model allowed researchers[10,11] to explain thrust and pressure oscillations in solid rocket motors.

Other works on flow induced in porous tubes indicated that acoustic oscillations could be driven by impingement of vortices that separate and develop in the vicinity of the injection wall. Dunlap et al.[12] characterized the fluctuating flowfield that develops along the length of a simulated cylindrical port rocket chamber. They described wall vortex formation and pairing, which give rise to shedding frequencies independent of the acoustic modes of the duct. In addition, results reported by Griffond et al.[13] defined theoretical criteria for wall vortex appearance and predicted unstable frequencies. Experimental investigations conducted by Avalon et al.[14] showed that self-sustained oscillations occur for characteristic depth-to-length ratios of the chamber and that wall velocity fluctuations can be linked to pressure fluctuations. The present studies were undertaken to investigate experimentally a flowfield in which two hydrodynamic instabilities occur, that is, shear layer vortex shedding and wall vortex shedding, in a porous wall confined chamber containing an obstacle. The setup was designed to simulate the main features of flowfields inside solid-propellant booster. Simultaneous analysis of pressure and velocity fluctuations were conducted to characterize the possible presence of self-sustained oscillations. Particularly, the two branches of the feedback loop are treated separately to describe best pressure and velocity field interactions and to show the influence of each unstable mechanism in the noise-generation phenomenon. Finally, an unbalanced mass flow rate between each side of the obstacle location has been found to be a very sensitive parameter to unstable flow behavior. A large-scale modification of

flow structure can occur due to the effect of wall injection boundary conditions.

II. Experimental Setup and Measuring Techniques

A. Test Channel

The experimental apparatus is a 1/40-scale model of the solid-propellant booster of Ariane 5. Complete details of the experimental system are described and relevant aspects of the geometry and data processing are given by Vetel et al.[15] The scale model did not completely reproduce the actual full-scale motor, but the latter was roughly similar through the presence of segmented blocks, wall injection, and submerged nozzle. In terms of internal design, the test channel was a 0.050-m-wide nonsymmetric two-dimensional channel. All other dimensions are specified in Fig. 1. As shown in Fig. 1, two injecting blocks were located in the chamber, and an obstacle was located between the two injecting blocks; the latter emerges above the porous walls. The flow was generated by injecting air at ambient temperature from a feeding unit whose mass flow rate could vary from 0.050 to 0.300 kg/s; the mass flow rate was estimated (±2%) by measuring the pressure drop caused by a diaphragm located downstream of the feeding unit. Injection into the channel was carried out through a porous wall mainly characterized by a sintered-bronze sphere Poral plate with 2-μm characteristic diameter and a flexible metallic woven sieve set at 10 mm above the Poral plate. The uniformity of the mass flow rate distribution along the porous wall was controlled by an accurate feeding system. For each injecting block, airflow was fed into a general manifold divided into 10 flexible polyamide tubes. In turn, these tubes fed an isolated cell, and the mass flow rate in each injection cell was controlled by sonic air inlets. The role of each isolated cell was to feed a given Poral plate area, where assumption of uniformity has been previously verified.[16] The Poral plate enabled us to isolate the flow in the chamber while the metallic woven sieve significantly reduced the injected turbulence in the chamber. Because of the metallic woven sieve, a significant decrease of the injected turbulence from 10% to a level lower than 4% could be obtained. A nozzle with sonic throat was located at the rear end of the chamber to ensure the acoustic isolation of the channel from the exterior environment. Every experimental run presented hereinafter was realized with a sonic nozzle condition. The height of the nozzle throat h_t could be varied, thereby controlling the mean Mach number M in the chamber. When our study was focused on the effect of dynamic conditions, one of the main parameters was the Reynolds number Re, which was expressed as a direct function of the injected mass flow rate. Internal velocity was then considered, and with the assumption of a constant injected mass flow rate, that is, a fixed Reynolds number, the nozzle throat was progressively closed or opened by stages at intervals of 0.05 mm to modify the Mach number level.

B. Measurement Techniques

Mean pressure and its fluctuating component were measured at the head end with a 7261 Kistler piezoelectric quartz transducer with a worse-case static pressure accuracy of 10 Pa. The dynamic response provides a fluctuating pressure sensitivity of about 0.02 Pa. Its 33-mm diam allows one to adapt the transducer via a flush mounting at the head end. Acquisition and analysis of the data (more than 200,000 samples) at 10-kHz frequency made it possible to determine the mean pressure level, the standard deviation, and the spectral content in the pressure field. Spectral analysis decomposition was performed with 4096 data blocks with 2.44-Hz frequency resolution and a spectral accuracy of about ±2.5%. The same control was applied to the velocity signals, measured by a Dantec 5-μm single miniature probe and a 5-μm X miniature probe. The frequency response of the hot-wire system was found to be approximately 100 kHz, and data were analyzed with a relevant calibration. The velocity–voltage relationship was assumed to follow a fourth-order polynomial. The calibration procedure required variation of velocities and inclination angles. There were 28 velocities covering the entire anticipated range chosen, and at each velocity, the probe was yawed 17 times to cover the angles from −40 to +40 deg. Thus, because of the hot-wire calibration equation and data acquisition, the uncertainty of the mean velocity was estimated to be equal to ±1% and that of the fluctuating velocity to ±2.5% (Ref. 17). Control of the injected air temperature was carried out by a K-thermocouple with a ±0.5-K accuracy, which allowed one to estimate the sound velocity a(±0.08%). Temperature, pressure, and velocity signals were recorded using an AT MIO-16E10 A/D board with a SC2040 submitting sampling data.

III. Hydrodynamic Instabilities of the Flow

A. Shear Layer Vortex Shedding

This work falls within the framework of a previous paper written by the authors.[15] As described in Ref. 15, a shear layer develops from the top of the obstacle by the mixing of the main flow with the wall injected flow through the second injecting block. Periodic shedding of vortices was observed, but additional measurements were made to identify clearly the unstable mechanisms involving in the shear layer oscillations. Figure 2a shows the spectral distribution of the u' fluctuating velocity component at several positions in the Y direction at $X = 0.1$, that is, close to the obstacle location. Under dynamic conditions ($M = 0.06$ and $Re = 0.86 \times 10^5$), spectra show one single peak at about 240 Hz, whatever the Y location. This dominant frequency is particularly pronounced in the high-speed region and the low-speed region of the shear layer, but disappears in the vicinity of the obstacle height, $Y \approx 0.36$. To check as to whether velocity oscillations at 240 Hz were consistent with periodic vortical flow, specific measurements were carried out. As described in Fig. 2b, one hot wire was held fixed in the upper region of the shear layer, $Y = 0.52$, while another was moved transversely from this position in the wall injection direction. The cross-power spectra were then calculated for several transverse locations of the moving probe. Figure 2b shows the magnitude $|s_{u'_1 u'_2}|$ (±2%) and phase $\theta_{u'_1 u'_2}$ (±2 deg) of cross-power spectra at 240 Hz as a function of the Y location, as well as the profile of turbulence intensity It. The magnitude of the cross power was relatively high when both wires were in the high-speed region of the shear layer and the phase angle between the two velocity signals was quite low. For $Y < 0.45$, the cross-power magnitude drops rapidly, and the phase angle increases significantly. Then, as Y decreases, the magnitude increases, and the phase angle approaches 180 deg, which indicates that axial velocity fluctuations in the high-speed region and the low-speed region of the shear-layer are in antiphase. The minimum in

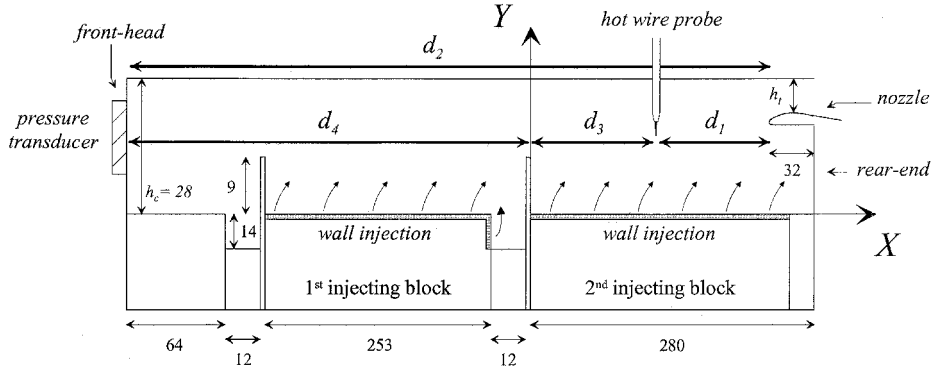

Fig. 1 Experimental configuration; all sizes are in millimeters.

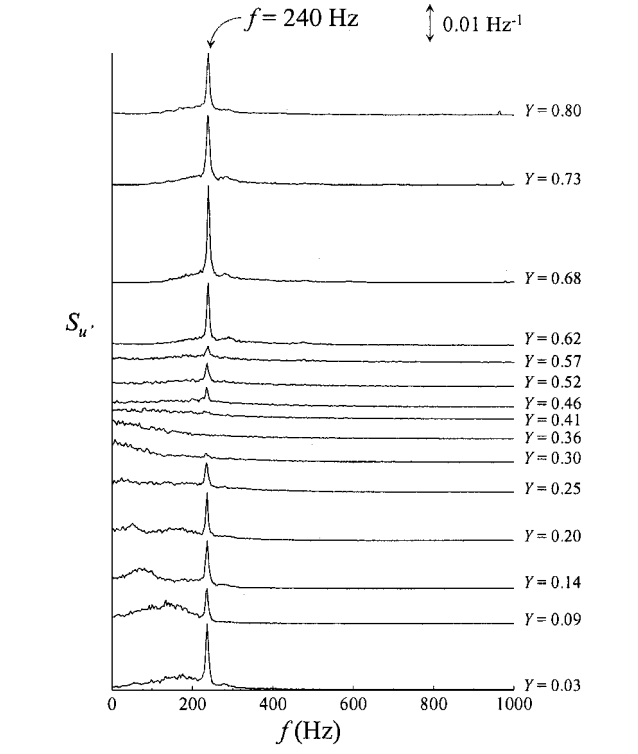

a)

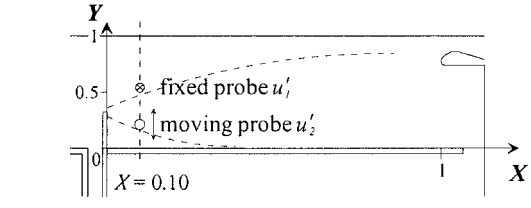

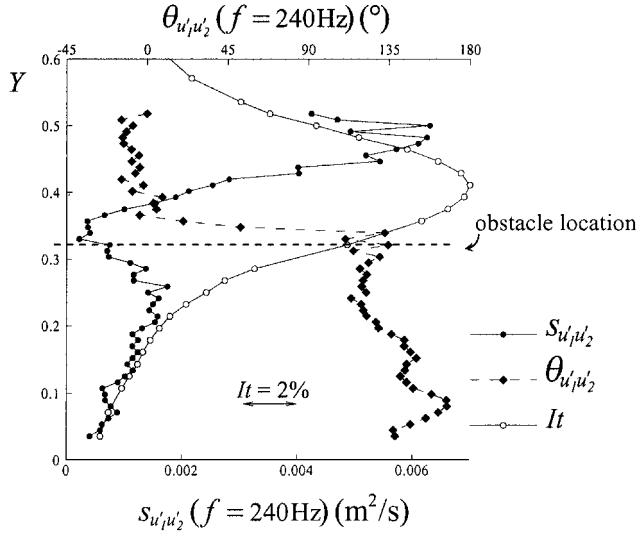

b)

Fig. 2 Velocity spectra near the obstacle location and cross power at 240 Hz.

the cross-power magnitude and the phase change occur near the Y location of the top of the obstacle, which is located under the maximum of the turbulence intensity It at this X location. Therefore, vortices are periodically shed at 240 Hz, and a measure of velocity fluctuations in the high-speed region of the shear layer suffices to estimate the frequency at which vortex shedding occurs.

Experiments then were conducted by changing the dynamic conditions of the flow; Fig. 3 shows the evolution of the predominant frequency of velocity spectra with regard to the Mach number M and are parameterized by several Reynolds numbers. Velocity fluctuations were measured in the high-speed region of the shear layer, that is, in a location higher than the maximum turbulence intensity location for two axial locations: 1) in the vicinity of the obstacle position ($X = 0.16$ and $Y = 0.52$) and 2) at the rear end of the chamber ($X = 0.64$ and $Y = 0.75$). For the first location, two general trends can be pointed out, regardless of the Reynolds number. First, it can be seen that the peak observed in Fig. 2a at $M = 0.06$ strongly depends on dynamic conditions because its frequency increases linearly with the Mach number. Thus, this frequency f_n corresponds to the natural instability of the shear layer generated in the wake of the obstacle. Second, for $M > 0.08$, spectra are characterized by several frequencies. In the Mach number range $0.08 < M < 0.13$, for instance, the natural shedding of vortices is accompanied by the excitation of the shear layer at another lower frequency. The latter also increases linearly but remains in the vicinity of the first longitudinal acoustic mode f_{1L} of the chamber; a response of the shear layer to the acoustics of the chamber in then observed. Indeed, the confined chamber acts as a resonator where the resonance frequencies match up with the closed–closed theoretical longitudinal acoustic modes f_{nL}. For $M > 0.11$, the different acoustic modes from f_{2L} to f_{4L} appear in the velocity spectra. Hence, the initial development of the shear layer shows a well-organized flow pattern on its own hydrodynamic instability with a response to the first four acoustic modes. Similar measurements have been performed for the second location studied downstream from the obstacle location, and Fig. 3 shows significant changes in the velocity fluctuations. Despite the natural instability observed for $M < 0.08$, as well as the response of the shear layer to the f_{1L} mode for $M < 0.13$, the appearance of the other acoustic modes has disappeared. That said, other trends are clearly observed: Three frequency stages in the vicinity of the first acoustic mode appear. For each of them, the frequency increases linearly with the Mach number until a jump that results in a lower value, and then another linear increase begins. Moreover, each of these three frequency stages matches up closely to the first three subharmonics of the fundamental hydrodynamic frequency f_n. Therefore, these results indicate that vortex pairing occurs between the separation point of the shear layer and the rear end of the chamber as observed in free shear flows at low- or high-speed exit velocities.[18,19] Shear layer behavior is then characterized by formation of vortices at its natural unstable frequency f_n modulated by an acoustic mode f_{nL} of the chamber. Consequently, a pairing phenomenon occurs, which forces the highest unstable frequencies to align with a frequency f_n/n close to f_{1L}.

B. Wall Vortex Shedding

Figure 4a presents a transverse distribution of axial velocity spectra at location $X = 0.80$ ($Re = 0.86 \times 10^5$ and $M = 0.09$). For small values of Y close to the injecting wall, fluctuations are characterized by a broadband spectrum centered around a frequency peak. When the probe is moved in the positive Y direction, energy contained in the frequency broadband decreases, and low-frequency energy increases. Close to the midheight of the chamber, $Y \approx 0.46$, a particular peak is no longer observed. Therefore, velocity fluctuations show a broadband spectra when recording in the vicinity of the wall. Spectral response with such a relatively large range of frequencies is well-known in high-speed turbulent jets[20] and in the wake of cylinders.[21] The latter was identified as consistent with a nearly regular array of vortices whose natural shedding frequency is not stationary but slightly deviates from a mean. To confirm whether or not this trend holds in the present experiment, the measurements carried out in the vicinity of the injecting wall were similar to those performed in the shear layer (Fig. 2b). Nevertheless, the phase angle relationship cannot be extracted from cross-power spectra because velocity fluctuations are not centered on any one single peak. Thus, this phase angle was approached with cross-correlation calculations between a velocity signal measured at a fixed probe far away from the wall injection, $Y = 0.46$, and a signal from a second probe moving from this position toward the wall injection. Figure 4b shows temporal cross-correlation coefficients between the two velocity signals as a function of r, which is the ratio of the distance between the two probes to the channel height h_c. When the probes are close

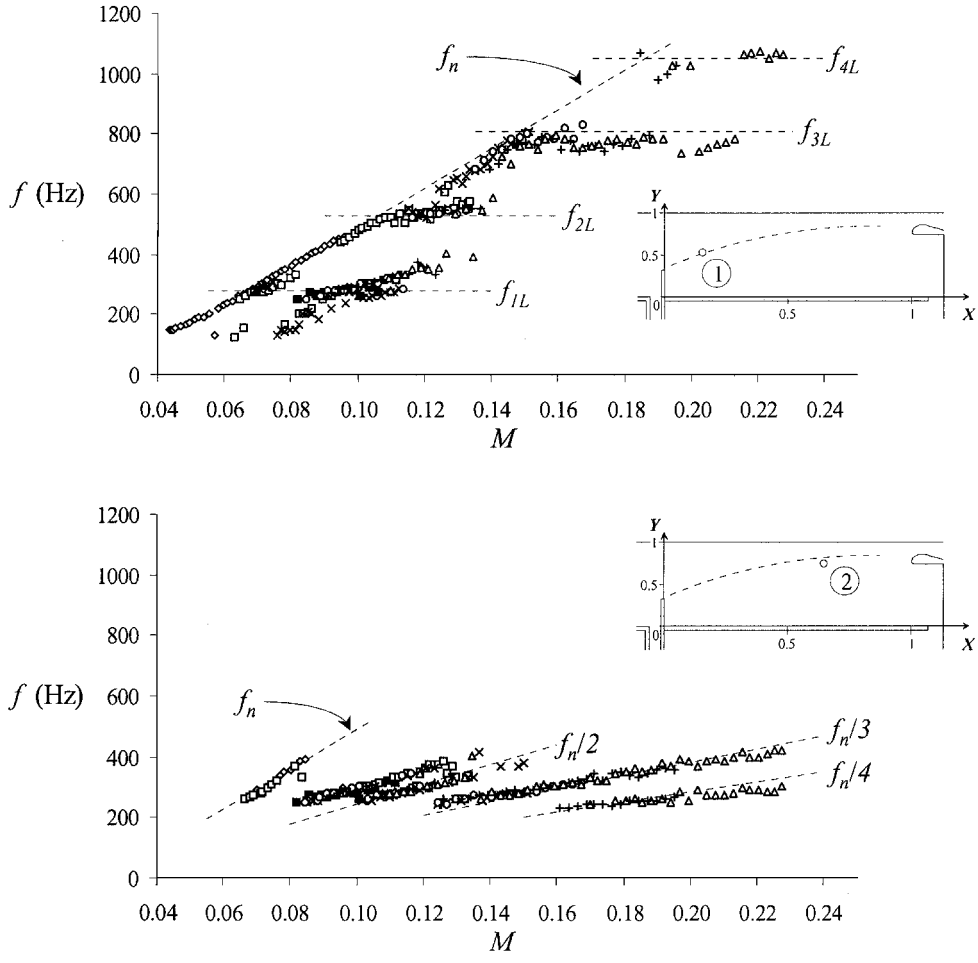

Fig. 3 Main frequencies of velocity spectra versus M with regard to Reynolds number Re level: 1) near the obstacle and 2) in the rear end of the chamber: ◇, $Re = 0.86 \times 10^5$; ■, $Re = 0.96 \times 10^5$; □, $Re = 1.14 \times 10^5$; ×, $Re = 1.29 \times 10^5$; ○, $Re = 1.45 \times 10^5$; +, $Re = 1.62 \times 10^5$; and △, $Re = 1.94 \times 10^5$.

to each other, $r = 0.01$, the maximum of $R_{u'_1 u'_2}$ occurs near $\tau = 0$, which shows that the axial velocity fluctuations are essentially in phase. As r increases, the peak correlation moves to increasing magnitudes of time delay, which reach a quadrature situation at around $r = 0.25$. Beyond this transverse location, the curves go through an inversion and retrace the phase changes in the inversion form. For the larger value of r presented, that is, for the moving wire close to the porous wall, velocity fluctuations are out-of-phase. Thus, these results are consistent with the hypothesis of vortices that separate and develop along the wall injection.

To estimate the influence of dynamic conditions on wall vortex shedding frequencies, Fig. 5 shows the change of velocity spectra with regard to the Mach number for three Reynolds numbers. Whatever the Reynolds number level, similar behavior is observed; the involved frequencies increase as a function of Mach number. Moreover, the centered frequency increases linearly with the Mach number, which seems to indicate that the vortex shedding phenomenon is mainly driven by a natural hydrodynamic frequency. Furthermore, as observed for velocity fluctuations in the shear layer, the Reynolds number does not affect the excited frequencies, which depend only on the Mach number. However, the increase of the Mach number has an effect on the depth of the broadband; the higher the velocity level, the larger the frequency band, raising the energy distribution on larger frequency scales.

C. Effects on Pressure Field

A resonance phenomenon in a confined chamber may enhance a high level of oscillations in the flow when velocity and pressure fluctuations align with each other. Thus, hydrodynamic instabilities are responsible for acoustic emission, and a feedback phenomenon takes place. To demonstrate the presence of such a coupling, Fig. 6 shows the spectral response of the shear layer in the wake of the emerging obstacle ($X = 0.64$ and $Y = 0.71$) and in the wall flow in the rear end of the chamber ($X = 0.98$ and $Y = 0.07$) with regard to Mach number level for $Re = 1.62 \times 10^5$.

Figure 6 allows one to compare these spectra with the spectral response of the head-end pressure fluctuations. All of the frequency stages in velocity spectra generated by vortex merging are exactly reproduced in the evolution of pressure fluctuations in the vicinity of the first longitudinal acoustic mode. This comparison clearly reveals the influence of vortex dynamics on pressure field; through impingement of vortices on the nozzle localized in the rear end of the chamber, pressure waves are generated and amplified by the confinement of the chamber. In addition, it was obvious from Fig. 3 that pressure oscillations had a strong influence on shear layer fluctuations at separation with appearance of longitudinal acoustic mode frequencies in the velocity response at the top of the obstacle. However, another trend can be observed in pressure field behavior. By the increase of the Mach number, the first four acoustic modes are excited. For example, the f_{1L} mode is the most excited frequency for $M < 0.1$, and up to this level, the second acoustic mode f_{2L} becomes the predominant frequency. A transition from f_{2L} to f_{3L} occurs at $M \approx 0.14$, and the f_{4L} mode appears for $M > 0.18$. This selective excitation of acoustic modes from the fundamental one to its first three harmonics could be linked to the velocity fluctuations measured near the injecting wall (Fig. 6). One can then make the assumption that the wall vortex shedding phenomenon acts by selecting the acoustic mode at which resonance occurs.

Correlation measurements between the fluctuating velocity and the fluctuating pressure were introduced in an attempt to evaluate the influence of one on the other. Figure 7a presents a characteristic $R_{u'p'}$ correlation coefficient (±1%) computed with velocity fluctuations recorded in the shear layer at ($X = 0.64$ and $Y = 0.71$) for $M = 0.18$. The change of $R_{u'p'}$ with regard to the time delay τ allows one to

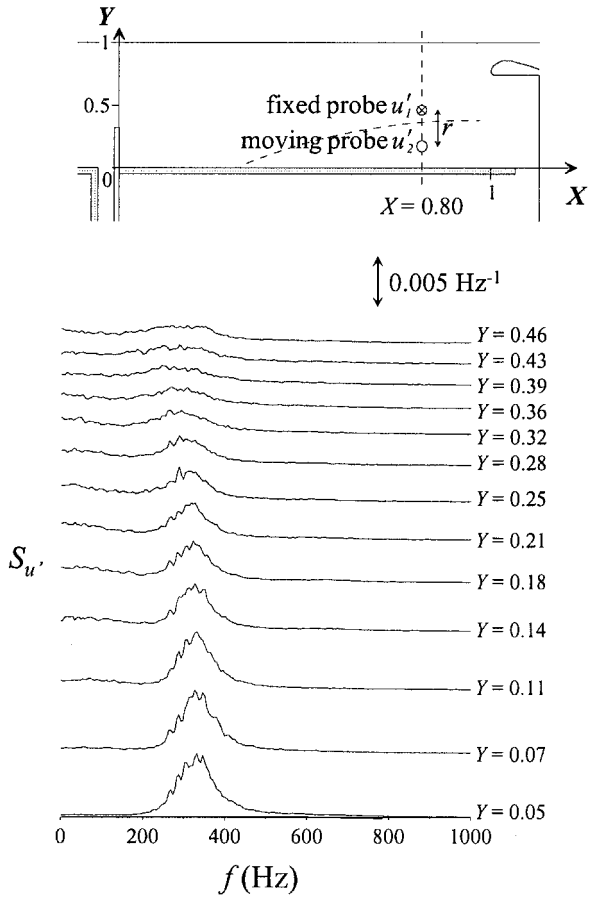

Fig. 4a Velocity spectra near the wall vs Y.

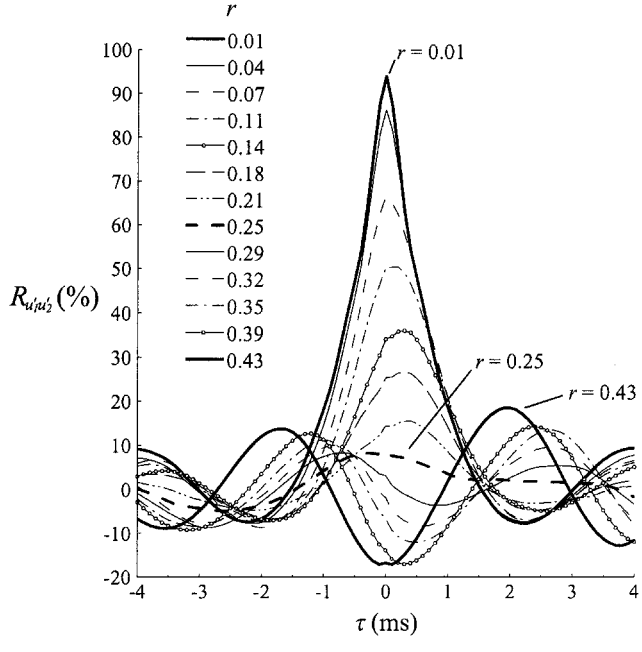

Fig. 4b Cross-correlation coefficients vs τ.

observe clearly the emergence of two peaks at which the correlation levels are significant. An analytical model proposed by Vetel et al.[22] satisfactorily explained these two peaks. The first, associated with a negative time delay τ^-, underlines the first branch of the feedback loop: a pressure wave creates a forced oscillation in the shear layer resulting in the formation of a coherent eddy and then continues its propagation up until the head end of the chamber. The second peak, associated with a positive time delay τ^+, represents the other branch of the feedback loop, that is, the generation of sound by vortex impingement on the nozzle.

Additional results are also plotted on Fig. 7a. In fact, because vortex merging implies frequency changes in the shear layer between separation and impingement, the same pressure and velocity signals were filtered to estimate the influence of the fundamental resonance frequency f_{1L} on the feedback phenomenon using a low-pass filter, as well as of all harmonics using a high-pass filter. The cutoff frequency of the filter was chosen to be the half-frequency of the f_{1L} and f_{2L} modes. The new results show that minor changes occur for the τ^- peak; the $R_{u'p'}$ level for low-pass filtered signals appears to be slightly lower than the one for raw signals, which in its turn is slightly lower than that reached by applying the high-pass filter. Indeed, the response of the shear layer is sensitive to all modes, and the f_{1L} mode is the least excited in the pressure field. On the contrary, an inverse trend is clearly shown for positive time delay τ^+. Even if using a high-pass filter slightly decreases the $R_{u'p'}$ peak correlation, the $R_{u'p'}$ level is greatly increased when the velocity signals are filtered with a low-pass filter reaching levels up to 20%. This result shows that noise generation by impingement of the shear layer on the nozzle occurs mostly around frequencies close to the f_{1L} mode, which is in agreement with the presence of frequency stages in the first acoustic mode behavior in pressure and velocity spectra of Fig. 6.

Correlation coefficients were also estimated with velocity fluctuations recorded close to the injecting wall ($X = 0.98$ and $Y = 0.07$) for the same Mach number (Fig. 7b). It is obvious that, whatever filter was employed, a strong τ^+ correlation is observed with a level higher than 50%. Therefore, wall vortex shedding contributes to generate pressure waves, and the high $R_{u'p'}$ level reached clearly demonstrates that wall instability is the predominant noise source. Spectra of pressure oscillations have actually shown that most of the energy is concentrated on harmonic modes, whereas the f_{1L} mode, for which the coupling phenomenon occurs, contributes to only a small part of the pressure fluctuation signal. Furthermore, characteristic frequencies of wall vortex shedding increase with regard to the Mach number, thereby implying the selectivity process of the excited modes. That said, wall velocity spectra in Fig. 6 showed the presence of two frequency stages for $M > 0.14$.

Figure 7b may provide further information on this point; no correlation at negative time delays is observed for raw and high-pass filtered signals; yet, with the low-pass filter, a peak appears, which indicates that receptivity of wall velocity fluctuations is detectable at the f_{1L} frequency. Compared with the distribution of velocity spectra (Fig. 6), note that the two frequency stages occur when the characteristic frequency band of wall vortex shedding is out of range of the first acoustic mode. Thus, it appears possible to force wall vortex shedding by acoustic oscillations. As stated by Beddini[23] and Liou et al.,[24] a change of injection velocity strongly modifies flow transition in porous-walled duct flows and, in this way, the fluctuating flowfield structure.

IV. Influence of Boundary Conditions

To estimate the strength of the two oscillation sources, the mass flow rate between the two injecting blocks, that is, from one side of the obstacle to the other, was unbalanced. To do so, all experiments were conducted with a constant Reynolds number ($Re = 0.86 \times 10^5$), which implies a constant total mass flow rate, and the mass flow rate of each injecting block was modified. When q_1 is considered as the new mass flow rate injected through the first injecting block and q_0 is the mass flow rate of the same block without unbalanced flow, the boundary condition modification is quantified by the α parameter. One can evaluate general modifications of the flowfield due to these new boundary conditions. Figure 8 presents longitudinal mean velocity profiles normalized by the maximum velocity in each section for three different α levels and at a fixed Mach number $M = 0.096$. In the wake of the obstacle, a region of the flow in which shear is significant is pointed out for $\alpha = 0$. Nevertheless, velocity gradients weaken rapidly, and beyond $X = 0.40$, profiles are no longer modified and remain similar until the rear end of the chamber. One can see that when the mass flow rate through the first injecting block is increased, that is, for $\alpha = 15\%$, no significant changes occur because velocity profiles conform quite well with those obtained for the $\alpha = 0$ case. Unlike $\alpha = 0$ and 15%, velocity

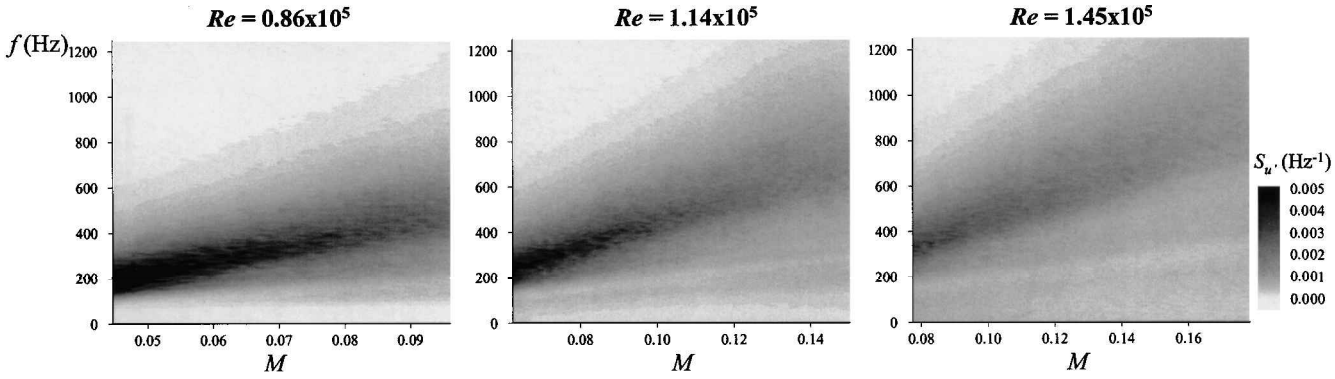

Fig. 5 Evolution of velocity spectra at wall ($X = 0.98$, $Y = 0.07$) with M.

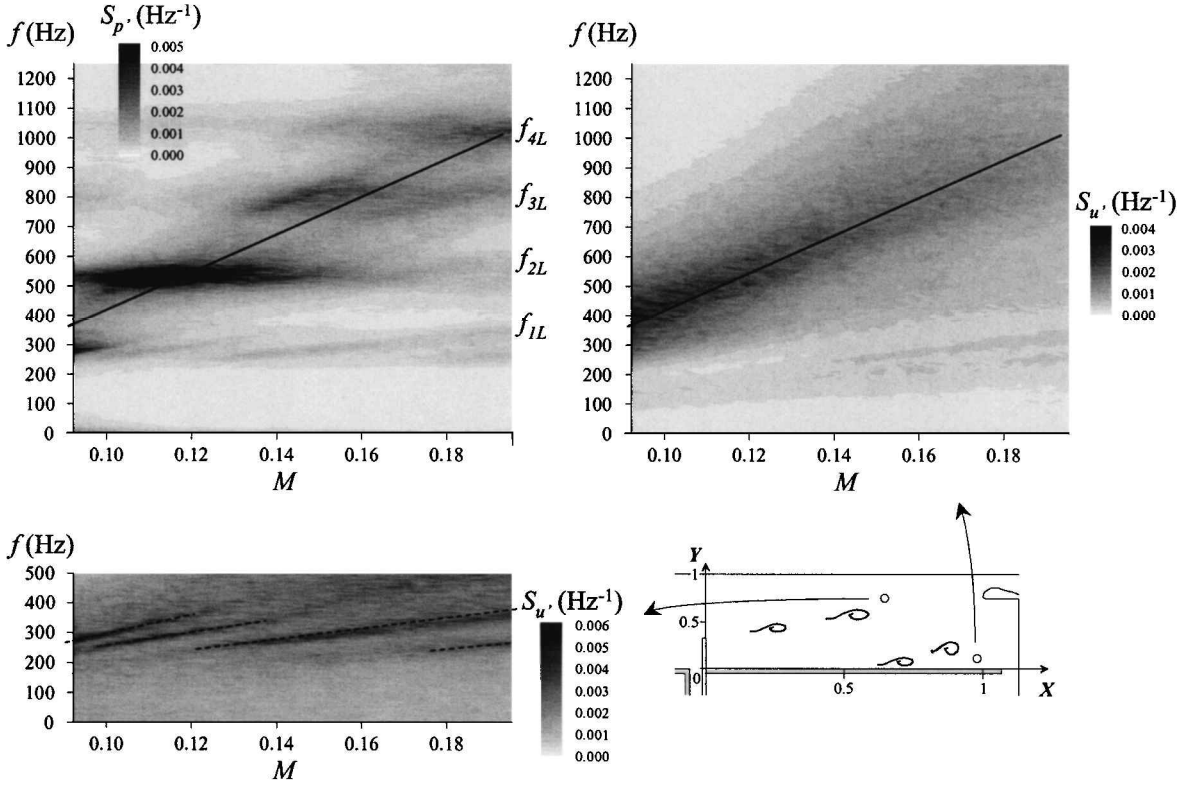

Fig. 6 Comparison of shear layer and wall vortex shedding with pressure spectra at the front head.

profiles are clearly modified when mass flow rate is smaller at the first injecting block ($\alpha = -15\%$). In fact, even if profiles at $X = 0.08$ and 0.16 are quite comparable, profile shape presents stronger gradients close to the injecting wall for $X \geq 0.24$. In this configuration, the velocity profile is continuously modified all along the chamber length to such a point that difference in the profile shape is observed for $Y \leq 0.4$. Therefore, it seems that a negative value of the α parameter affects the flowfield in the vicinity of the wall injection, whereas a positive value does not appear to modify the mean flowfield behavior. Thus, it can be interesting to study how the hydrodynamic instabilities of the flow are modified for the two α cases.

A. Positive α Case

The change of velocity fluctuation spectra with regard to the Mach number for $\alpha = 15\%$ are shown in Fig. 9 for the same two locations as those described in Fig. 3. At the first location close to the obstacle location (Fig. 9a), the presence of a natural vortex shedding frequency is detected with a linear evolution with the Mach number. Without boundary condition changes ($\alpha = 0$) indicated by dotted lines in Fig. 9a, it is obvious that the same instabilities are observed, but shear layer characteristic frequencies have changed. First, the natural frequency f_n is higher than the $\alpha = 0$ case; indeed, the velocity difference between the high-speed region and the low-speed region of the shear layer is higher than the $\alpha = 0$ case. Second, forced oscillations of the shear layer at the f_{1L} frequency appears for a lower Mach number, $M \approx 0.065$. Direct consequences of these changes can be seen for the second location studied (Fig. 9b), downstream from the obstacle location. As observed for the $\alpha = 0$ case, the natural frequency f_n has disappeared in the velocity spectra, whereas fluctuations occur at frequencies close to $f_n/2$ and $f_n/3$, which are in the vicinity of the first longitudinal acoustic mode. Pressure fluctuations spectra also shown in Fig. 9c are characterized by three successive stages, each of them described by a linear increase of the frequency around the f_{1L} mode. These frequency stages are then directly linked to the phenomenon occurring in the shear layer. Thus, by increasing the mass flow rate through the first injecting block, the pairing mechanism is favored, which underlines the presence of the coupling phenomenon between hydrodynamics and acoustics. Under these conditions, how does the wall vortex shedding behave, given such boundary condition modification?

Figure 10 compares spectra of velocity fluctuations recorded in the rear end of the chamber and close to the porous wall for the two α cases at $M = 0.9$. For $\alpha = 0$ (Fig. 10b), the spectrum involves a large frequency band centered around a given frequency. For $\alpha = 15\%$ (Fig. 10a), it can be seen that the frequency of the dominant peak increases, and the bandwidth of the excited frequency is

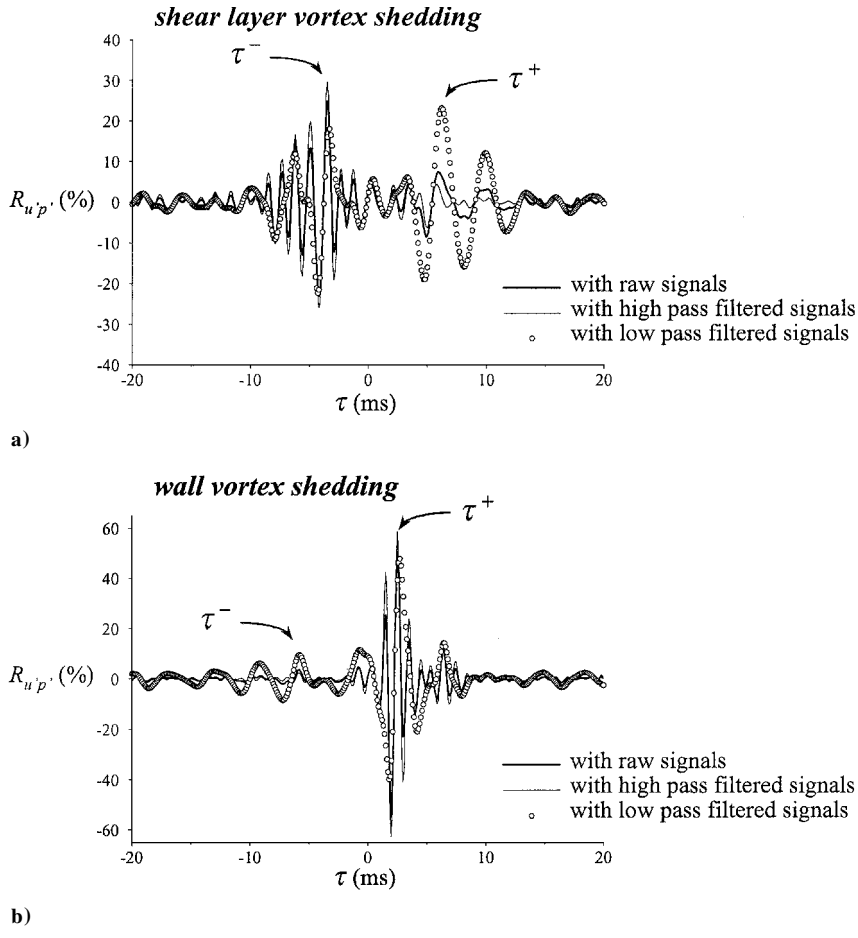

Fig. 7 Cross-correlation coefficients between pressure fluctuations and a) shear layer velocity fluctuations and b) wall velocity fluctuations.

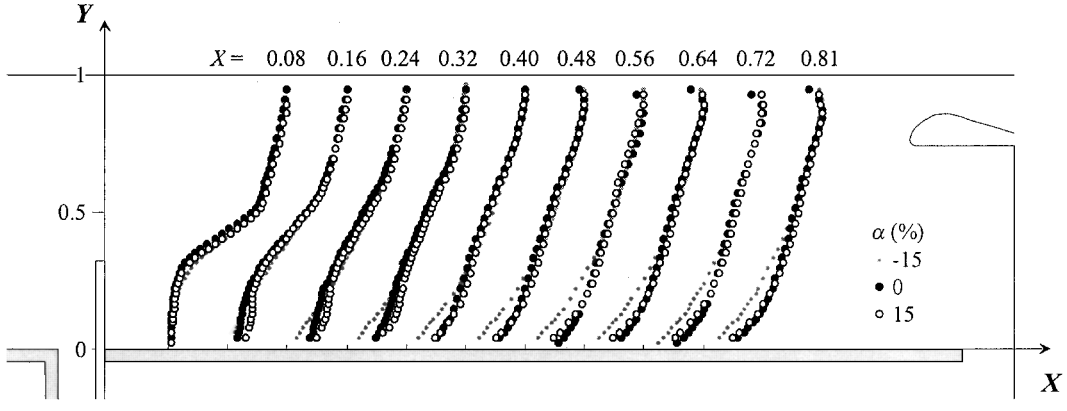

Fig. 8 Normalized longitudinal mean velocity profiles downstream from the obstacle location vs α.

larger. Moreover, excitation of low frequencies less than 300 Hz is observed, which indicates an intense turbulent behavior of the flowfield. Because the vortex peak becomes increasingly broad, the ability of wall vortex shedding to generate sound has been estimated with $R_{u'p'}$ calculations. A correlation is present at a positive time delay, which indicates that, as already seen (Fig. 7b), vortex development close to the injecting wall generates sound by impingement on the nozzle. Nevertheless, a significant difference is observed between the two cases on the $R_{u'p'}$ levels reached, 38% for $\alpha = 0$ (Fig. 10c) and only 15% for $\alpha = 15\%$ (Fig. 10d). From these results, the α parameter is significant on velocity–pressure interaction, which could alter noise generation by wall vortex impingement and affect the overall noise level.

Figure 11 shows the change of the nondimensional pressure fluctuations root-mean square with regard to the Mach number, and one can see that the noise generation is sensitive to the α value. For the nominal case, $\alpha = 0$, the evolution of $\sqrt{p'^2}/p$ with M can be described by a linear increase up to M approximately equal to 0.085, followed by a higher growth. When the mass flow rate is increased through the first injecting block up to 10%, a similar shape is followed by the mean pressure fluctuation level. However, for $\alpha = 15\%$, although wall vortex contribution is lower in sound generation, one can see that the overall noise level increases for $M > 0.08$. Then, with higher value of α, this tendency is confirmed with a much higher level whatever the Mach number is for the $\alpha = 25\%$ case.

The change in boundary conditions underlines a strong influence on flowfield behavior. On the one hand, wall vortex instability is altered, and consequently, noise generation is also altered; on the other hand, the vortex pairing occurring in the shear layer is favored. Therefore, the increase of the noise level observed indicates that an increase of the mass flow rate through the first injecting block tends to favor shear layer instability to the detriment of wall instability, in

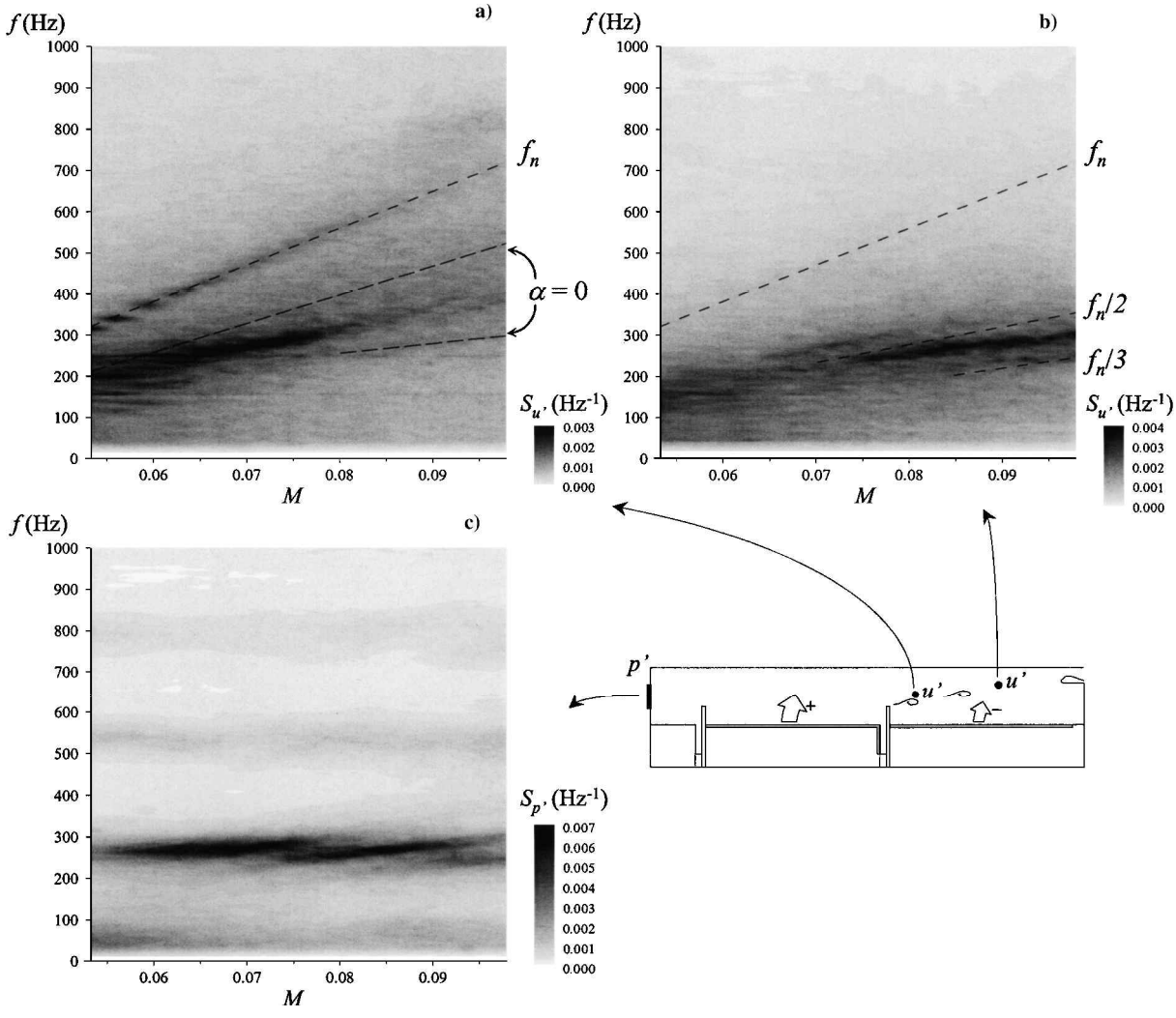

Fig. 9 Shear layer and pressure oscillation behavior vs M for $\alpha = 15\%$.

such a way that the shear layer instability becomes the predominant source of oscillation of the flow. Thus, it may be interesting to study flowfield organization by decreasing the mass flow rate through the first injecting block, that is, for negative values of the α parameter.

B. Negative α Case

Figure 12 presents spectra of wall velocity fluctuations ($X = 0.98$ and $Y = 0.07$) as a function of the Mach number for $\alpha = -15\%$. Wall vortex shedding is mainly characterized by broadband velocity spectra with a main frequency peak increasing linearly with Mach number; a similar trend was observed for the other studied α levels. However, unlike the $\alpha = 15\%$ case (Fig. 10), the involved bandwidth is much smaller than those observed for $\alpha = 0$ and 15%. Moreover, correlation coefficient $R_{u'p'}$ estimated at $M = 0.09$ reaches the level of 66%, which indicates a stronger influence of wall instability on the pressure field. Therefore, a negative value of α favors noise generation by wall vortex shedding, which is the trend opposite that observed for a positive value of α. Under these conditions, the shear layer response to such a behavior has been evaluated. Figure 13 shows the evolution of velocity spectra obtained for the two characteristic locations presented in Fig. 9. Close to the obstacle location, the decrease of mean velocity levels in the high-speed region of the shear layer induced by a decrease of the mass flow rate injected through the first injecting block provides a decrease in the slope of the natural frequency f_n linear evolution with Mach number (Fig. 13a). Consequently, this frequency appears to be lower than the f_{1L} mode for low Mach numbers but reaches the value of the first acoustic mode at $M = 0.08$. Then, for higher Mach numbers, several linear growths and jumps of the excited frequency are observed. Moreover, a similar behavior is observed at the other location studied (Fig. 13b), despite broadband background velocity fluctuations. Pressure fluctuations spectra, also shown in Fig. 13c, allow one to evaluate how the two instabilities act on the resonance phenomenon. First, for $M < 0.08$, the f_{1L} resonance is accompanied by linear evolution of a broadband frequency (from $f \approx 150$ Hz at $M = 0.053$ to $f \approx 280$ Hz at $M = 0.08$) emanating from the wall vortex shedding frequency influence (Fig. 13). Second, the influence of shear layer instability is also underlined by the presence of several frequency stages similar to those observed in the shear layer velocity fluctuations. Nevertheless, this behavior cannot possibly be due to vortex merging. Indeed, contrary to the $\alpha = 0$ and 15% cases, the frequency stages occur near the shear layer separation and, moreover, natural instability frequency are not high enough to provide subharmonic frequencies in the vicinity of the f_{1L} acoustic mode. Another mechanism is consequently responsible for this behavior. As first described by Rossiter,[9] the feedback loop can be expressed as follows:

$$mT = l/u_c + l/a(1 - M) \tag{1}$$

in which T is the vortex shedding period, l is the distance between shear layer initiation and impingement points, u_c is the convection speed of vortices, and m is to the number of vortices. The first term on the right-hand side of Eq. (1) represents the time for a vortex to travel from the shear layer formation to the impingement location, and the second term is the time for the acoustic pulse generated by vortex impingement to travel back until the shear layer initiation point, perturbing the velocity fluctuations to contribute to a subsequent vortex. If this feedback loop is responsible for the shear layer behavior observed here, an integer number of vortices should fit between the obstacle location and the nozzle location.[19,25]

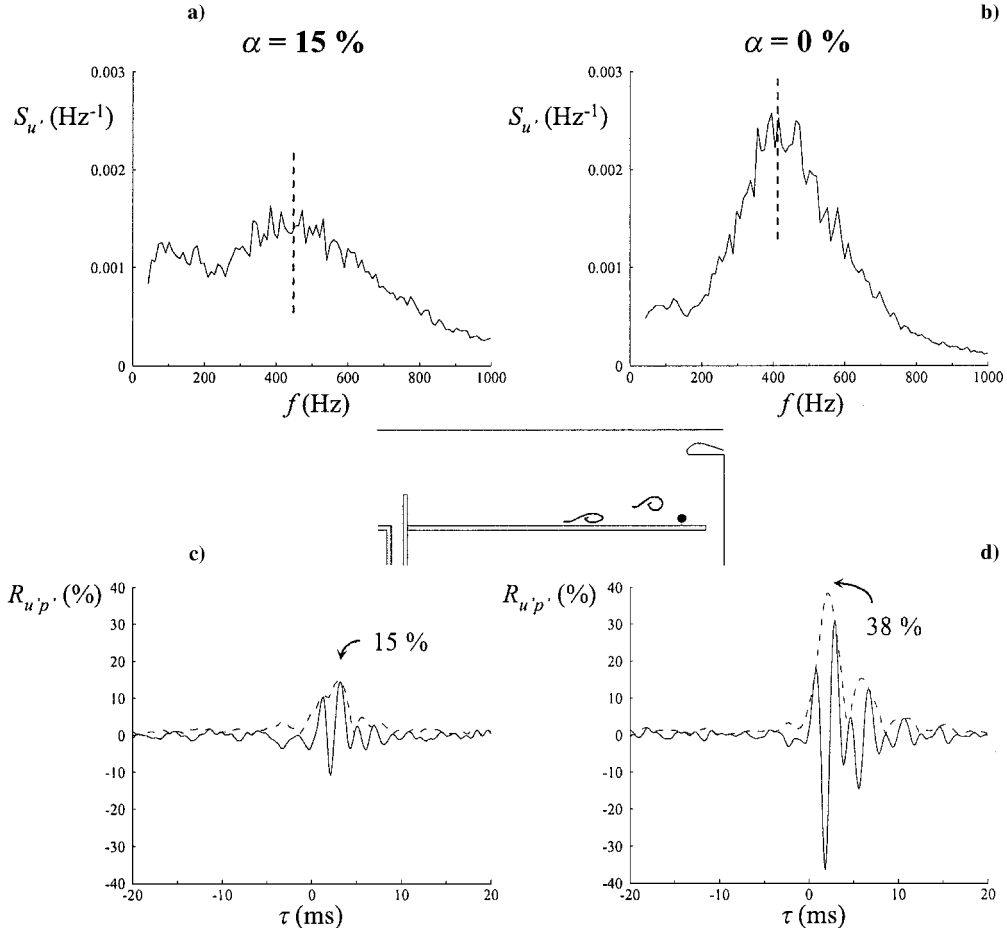

Fig. 10 Comparison of wall velocity spectra ($X = 0.98$, $Y = 0.07$) for two α cases and associated cross-correlation coefficients vs τ.

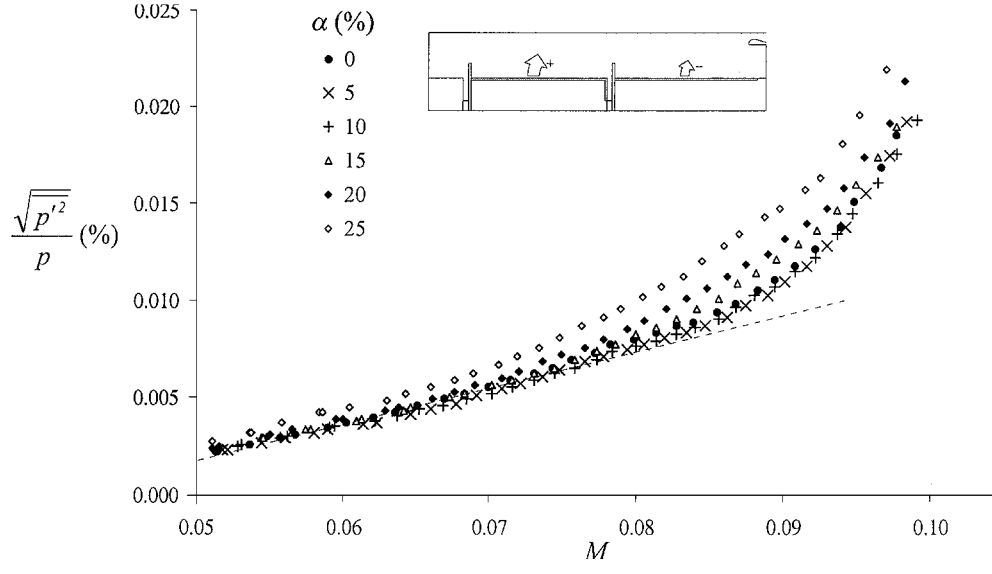

Fig. 11 Influence of positive α values on the normalized rms pressure fluctuations at the front head.

To check this assumption, values of m have been estimated for each frequency stage occurring in the velocity fluctuations. Therefore, the mean convection speed of vortices also needs to be estimated. The measure of u_c, nonetheless, remains difficult because the flowfield is quite complex, but this estimation can be deduced from the time delays τ^- and τ^+, which are expressed as[15]

$$\tau^+ = d_1 \big/ u_c^+ + d_2/a(1 - M) \tag{2}$$

$$\tau^- = -d_3 \big/ u_c^- + d_4/a(1 - M) \tag{3}$$

where u_c^- is the mean convection speed between the obstacle location and the velocity probe and u_c^+ the mean convection speed between the velocity probe and the nozzle location. Therefore, the mean convection speed between the obstacle location and the nozzle location can easily be obtained from

$$(d_1 + d_3)/u_c = d_1 \big/ u_c^+ + d_3 \big/ u_c^- \tag{4}$$

To obtain an estimation of u_c with high accuracy, correlation coefficient $R_{u'p'}$ has been calculated with velocity fluctuations recorded at $X = 0.64$ and $Y = 0.75$. This position actually provides satisfactory

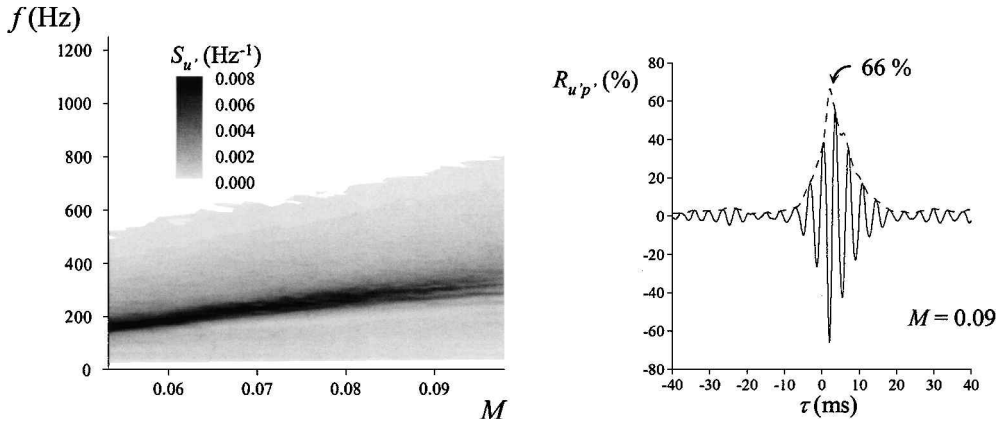

Fig. 12 Wall velocity spectra vs M and cross-correlation coefficient at $M = 0.09$ for $\alpha = -15\%$.

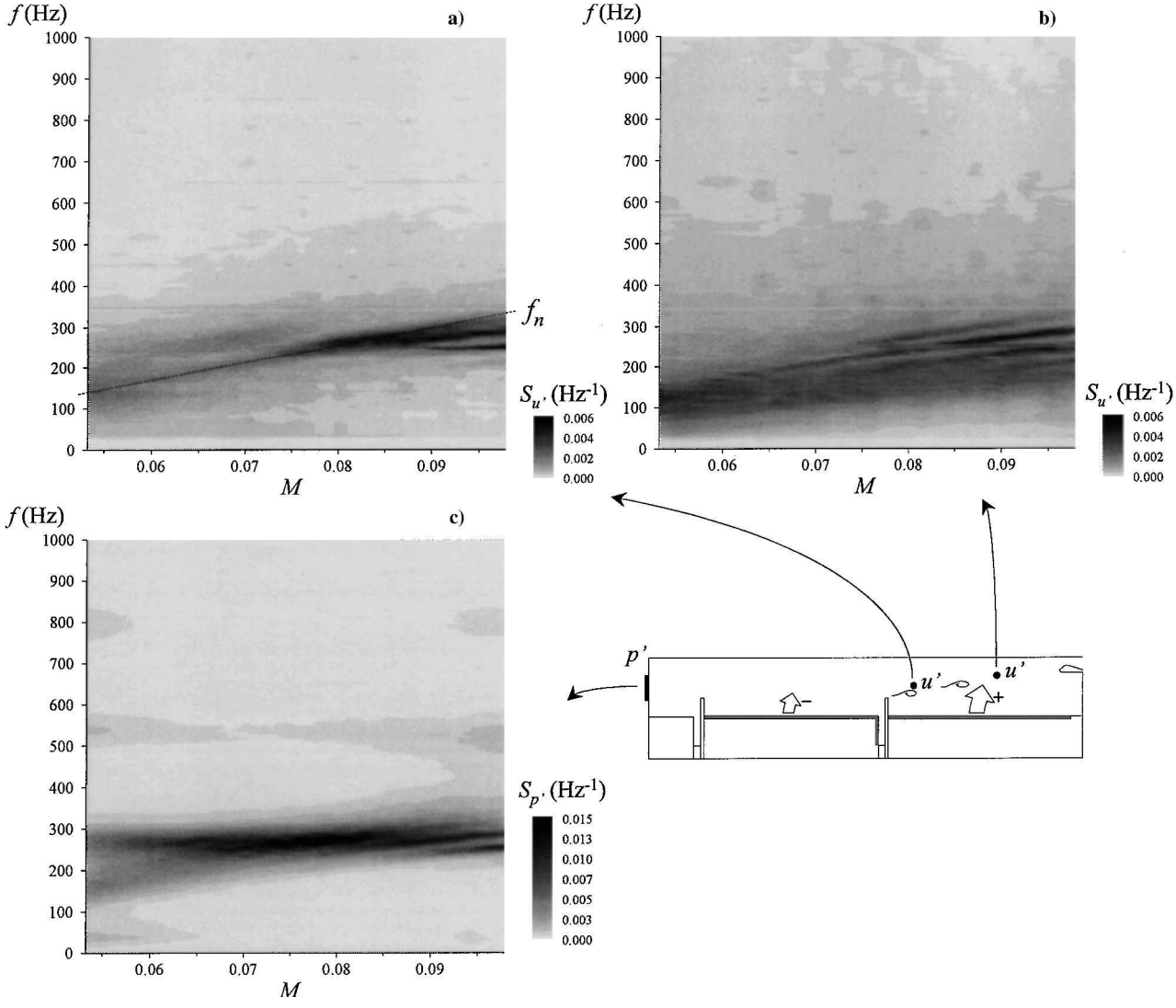

Fig. 13 Shear layer and pressure oscillation behavior vs M for $\alpha = -15\%$.

correlation levels for positive as well as negative time delays. As shown in Fig. 14, the existence of τ^- and τ^+ is strongly observed with $R_{u'p'}$ levels at about 20%, especially for $M > 0.7$, where velocity fluctuations begin to show frequency stage behavior, as seen in Fig. 13. Then, when Eqs. (2–4) are used, the convection speed is computed, and the mean convection Mach number $M_c = u_c/a$ is plotted in Fig. 14 as the Mach number increases. Observe in the linear evolution of M_c with Mach number that the ratio of the mean convection speed of vortices to the mean velocity of the flow reaches a constant value $M_c/M = 0.32$. Therefore, by use of Eq. (1), the values of m were estimated for each frequency stage, that is, for each oscillation period T. The results, also plotted in Fig. 14, show that, for all stages, m almost remains at a constant value whatever the Mach number is. Moreover, these values are close to an integer, from eight for the first stage to five for the fourth stage. For each oscillation stage, an integer number of vortices is then present between the shear layer initiation at the top of the obstacle and the nozzle location, spotlighting the vortex dynamic adaptation to follow the first resonance frequency, which underlines the presence of a strong coupling phenomenon between shear layer instability and pressure oscillations.

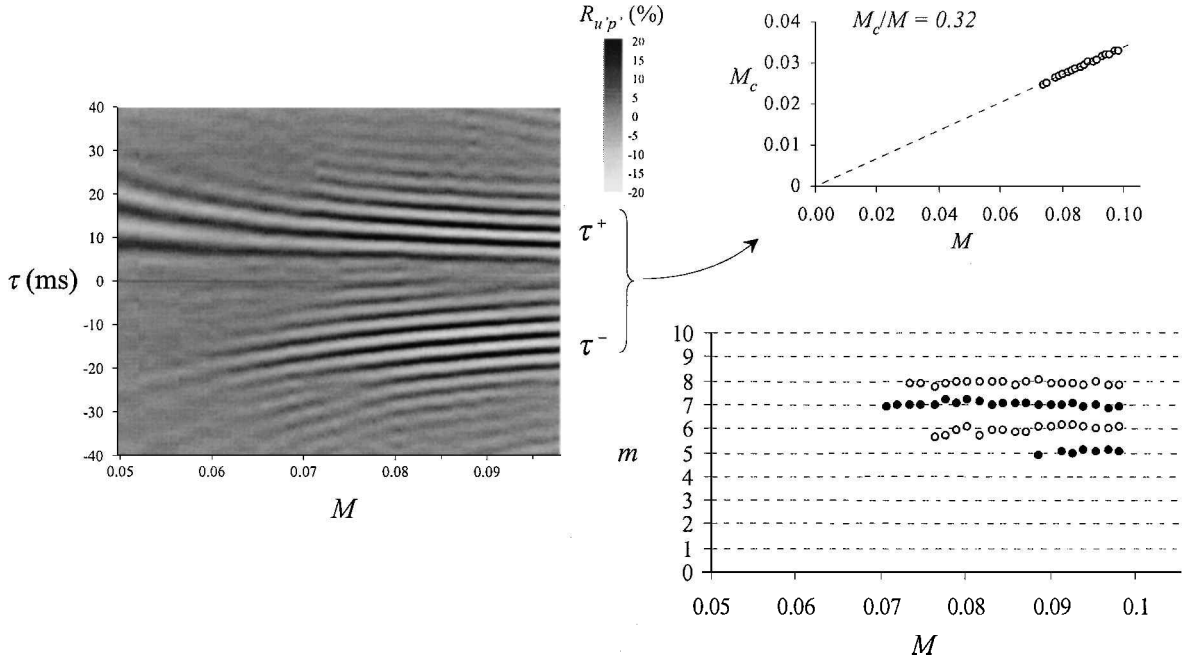

Fig. 14 Estimation of the convection speed of shear layer vortices and computed m values via cross-correlation coefficients vs M for $\alpha = -15\%$.

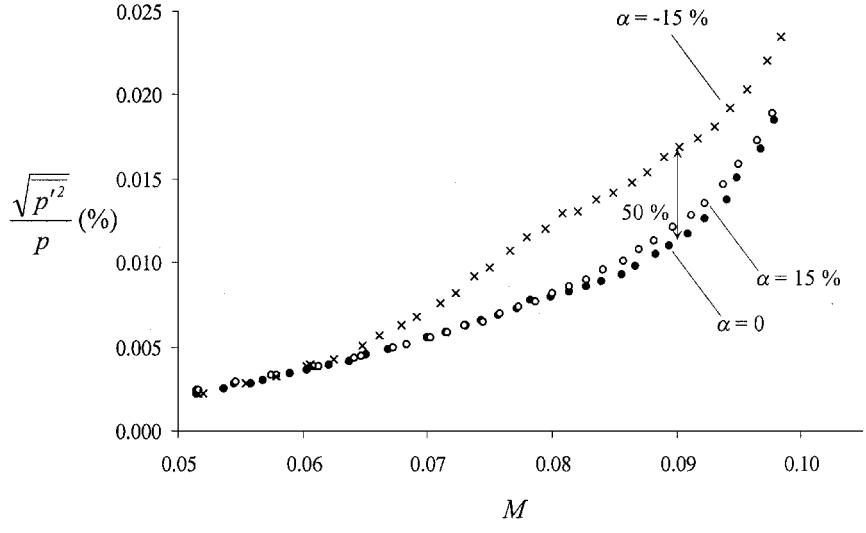

Fig. 15 Comparison of normalized rms pressure fluctuations at the front end for three values of α.

Thus, in the negative α case, and contrary to the positive α case, the two instabilities of the flowfield are amplified. This implies, as shown in Fig. 15, that the pressure fluctuation level drastically increases, reaching 50% more than the $\alpha = 0$ case at $M = 0.09$. It is once again evident that wall vortex shedding appears to be the main source of flow oscillation because its amplification contributes more to noise generation than does shear layer amplification.

V. Conclusions

Simultaneous pressure and velocity oscillation measurements in an injecting flow containing an emerging obstacle have shown two different hydrodynamic instabilities. Wall instability is identified as a natural instability of the flow induced by a porous wall, and impingement of wall vortices on the nozzle localized in the rear end of the chamber is responsible for pressure wave generation. The linear increase of the broadband wall vortex shedding frequencies with regard to the mean velocity level induces a resonance state and triggers the acoustic mode selectivity process. In addition, the shear layer generated at the top of the obstacle in the main flow is characterized by a coupling phenomenon where periodic vortex shedding frequencies organize in the vicinity of the first acoustic mode through vortex pairing mechanisms. Experiments conducted to destabilize the flow between each injecting blocks, that is, on either side of the obstacle, have shown different types of instability behavior. By the increase of the mass flow rate through the first injecting block, the shear layer coupling phenomenon is amplified to the detriment of wall vortex development. On the contrary, a decrease of the first injecting block flow rate implies amplification of the two instability sources of the flow. Moreover, the coupling phenomenon of the shear layer instability with acoustics is no longer described by vortex merging but by a modification of the number of vortices present at a given time between separation and impingement. Thus, these results underscore that a small unbalanced mass flow rate can imply a change of flow behavior and noise sources, as well as self-sustained oscillation mechanism.

The present results have shown the sensitivity of the unstable mechanisms with regard to the wall injection conditions. Nevertheless, it would be interesting to study whether a complete trigger of wall vortex shedding by pressure waves could appear by changing, for instance, the pseudoturbulence levels, that is, by changing the porous wall properties. In addition, if self-sustained oscillations appear at wall simultaneously with a shear layer coupling phenomenon, each unstable mechanism is able to drive pressure oscillations. Under such conditions, one instability could control the

other one. On the other hand, because the feedback loop characteristics are determined by velocity level and separation to impingement length, it may be possible to observe two self-sustained oscillation mechanisms if an adaptation of the longitudinal location of wall vortex appearance occurs.

Acknowledgments

This research was sponsored by the Centre National d'Etudes Spatiales (CNES). We give special thanks to Michel Pons, Director of the Solid Propulsion Department, for his tireless aid. These studies were performed within the framework of the "Aerodynamics of Solid Segmented Motors" research program of the CNES, concerning the Solid Propellant Motor/P230 of Ariane 5, and as a result of a research convention with the Office National d'Etudes et de Recherches Aérospatiales.

References

[1]Rockwell, D., and Naudasher, E., "Self-Sustained Oscillations of Impinging Free Shear Layers," *Annual Review of Fluid Mechanics*, Vol. 71, 1979, pp. 67–94.

[2]Rockwell, D., "Oscillations of Impinging Shear Layers," *AIAA Journal*, Vol. 21, No. 5, 1983, pp. 645–664.

[3]Hourigan, K., Welsh, M. C., Thompson, M. C., and Stokes, A. N., "Aerodynamic Sources of Acoustic Resonance in a Duct with Baffles," *Journal of Fluids and Structures*, Vol. 4, No. 4, 1990, pp. 345–370.

[4]Dunlap, R., and Brown, R. S., "Exploratory Experiments on Acoustic Oscillations Driven by Periodic Vortex Shedding," *AIAA Journal*, Vol. 19, No. 3, 1981, pp. 408, 409.

[5]Culick, F. E. C., and Magiawala, K., "Excitation of Acoustic Modes in a Chamber by Vortex-Shedding," *Journal of Sound and Vibration*, Vol. 64, No. 3, 1979, pp. 455–457.

[6]Flandro, G. A., and Jacobs, H. R., "Vortex Generated Sound in Cavities," AIAA Paper 73-1014, 1973.

[7]Schachenmann, A., and Rockwell, D., "Self-Sustained Oscillations of Turbulent Pipe Flow Terminated by an Axisymmetric Cavity," *Journal of Sound Vibration*, Vol. 72, No. 4, 1980, pp. 61–72.

[8]Tam, C. K. W., and Block, P. J. W., "On the Tones and Pressure Oscillations Induced by Flow over Rectangular Cavities," *Journal of Fluid Mechanics*, Vol. 89, No. 2, 1978, pp. 373–399.

[9]Rossiter, J. E., "Wind-Tunnel Experiments on the Flow over Rectangular Cavities at Subsonic and Transonic Speeds," Ministry of Aviation, Repts. and Memoranda 3438, Aeronautical Research Council, London, Oct. 1964.

[10]Scippa, S., Pascal, P., and Zanier, F., "Ariane 5 MPS Chamber Pressure Oscillations Full Scale Firings Results Analysis and Further Studies," AIAA Paper 94-3068, June 1994.

[11]Dotson, K. W., Koshigoe, S., and Pace, K. K., "Vortex Shedding in a Large Solid Rocket Motor Without Inhibitors at the Segment Interfaces," *Journal of Propulsion and Power*, Vol. 13, No. 2, 1997, pp. 197–206.

[12]Dunlap, R., Blackner, A. M., Waugh, R. C., Brown, R. S., and Willougby, P. G., "Internal Flowfield Studies in a Simulated Cylindrical Port Rocket Chamber," *Journal of Propulsion and Power*, Vol. 6, No. 6, 1990, pp. 690–704.

[13]Griffond, J., Casalis, G., and Pineau, J.-P., "Spatial Instability of Flow in a Semi Infinite Cylinder with Fluid Injection Through Its Porous Walls," *European Journal of Mechanics. B, Fluids*, Vol. 19, No. 1, 2000, pp. 69–87.

[14]Avalon, G., Casalis, G., and Griffond, J., "Flow Instabilities and Acoustic Resonance of Channels with Wall Injection," Joint Propulsion Conf. and Exhibit, AIAA/American Society of Mechanical Engineers/American Society for Engineering Education, July 1998.

[15]Vétel, J., Plourde, F., and Doan-Kim, S., "Mixing Effects Between Self-Sustained Oscillations and Unstable Hydrodynamic Behavior near Injecting Walls," *AIAA Journal*, Vol. 39, No. 8, 2001, pp. 1455–1468.

[16]Couton, D., Plourde, F., and Doan-Kim, S., "Cold Gas Simulation of a Solid Propellant Rocket Motor," *AIAA Journal*, Vol. 34, No. 12, 1996, pp. 2514–2522.

[17]Yavuzkurt, S., "A Guide to Uncertainty Analysis of Hot-Wire Data," *Journal of Fluids Engineering*, Vol. 106, 1984, pp. 181–186.

[18]Ho, C. M., and Huang, L. S., "Subharmonics and Vortex Merging in Mixing Layers," *Journal of Fluid Mechanics*, Vol. 119, 1982, pp. 443–473.

[19]Ho, C. M., and Nosseir, N. S., "Dynamics of an Impinging Jet. Part 1: The Feedback Phenomenon," *Journal of Fluid Mechanics*, Vol. 105, 1981, pp. 119–142.

[20]Lau, J. C., Fisher, M. J., and Fuchs, H. V., "The Intrinsic Structure of Turbulents Jets," *Journal of Sound and Vibration*, Vol. 22, No. 4, 1972, pp. 379–406.

[21]Blevins, R. D., "The Effect of Sound on Vortex Shedding from Cylinders," *Journal of Fluid Mechanics*, Vol. 161, 1985, pp. 217–237.

[22]Vétel, J., Plourde, F., and Doan Kim, S., "Influence of Hydrodynamic Conditions on the Vortex Shedding Phenomenon," AIAA Paper 2000-2000, June 2000.

[23]Beddini, R. A., "Injection-Induced Flows in Porous-Walled Ducts," *AIAA Journal*, Vol. 24, No. 11, 1986, pp. 1766–1773.

[24]Liou, T. M., Lien, W. Y., and Hwang, P. W., "Transition Characteristics of Flowfield in a Simulated Solid-Rocket Motor," *Journal of Propulsion and Power*, Vol. 14, No. 3, 1998, pp. 282–28.

[25]Nomoto, H., and Culick, F. E. C., "An Experimental Investigation of Pure Tone Generation by Vortex Shedding in a Duct," *Journal of Sound and Vibration*, Vol. 84, No. 2, 1982, pp. 247–252.

W. J. Devenport
Associate Editor